AIAA SciTech Forum
23-27 January 2023, National Harbor, MD & Online
AIAA SCITECH 2023 Forum

10.2514/6.2023-1478

Multi-Fidelity and Multi-Disciplinary Design Optimization of A Low-Boom Supersonic Transport Aircraft

Melike Nikbay *
Istanbul Technical University, Astronautical Engineering Department, Maslak, Istanbul, 34469, Türkiye

Dilan Kilic†, Enes Cakmak‡, Huseyin Emre Tekaslan §, Sihmehmet Yildiz¶, Yusuf Demiroglu‖
Istanbul Technical University, Maslak, Istanbul, 34469, Türkiye

The purpose of this study is to demonstrate the conceptual design of a low-boom supersonic transport aircraft by utilizing multi-fidelity and multi-disciplinary design optimization techniques. The research group aims to set forth a commercial supersonic aircraft model for future benchmarking studies. The presented multi-disciplinary design framework coherently incorporates aerodynamic, aeroelasticity and sonic boom prediction solvers into the design process. In the multi-fidelity modelling approach, the rigid flow solution is chosen to be the low-fidelity model while the aeroelastic flow solution is used as the high-fidelity model. For aerodynamic and fluid-structure interaction (FSI) solutions, the SU2 open-source suite is employed. For sonic boom prediction, NASA's sBOOM code is coupled with the SU2 code's output pressure data using in-house Python scripts. The parametric geometric modelling is achieved by using the ESP (Engineering Sketch Pad) program. In the multi-fidelity optimization study, the in-house coKriging and genetic algorithm codes of ITU AeroMDO Lab are used for multi-fidelity surrogate modelling and optimization studies, respectively. A 8.48% reduction in PLdB (perceived loudness in decibels) is achieved by the current shape optimization process for a commercial supersonic aircraft model with a complex geometry.

I. Introduction

Low-boom supersonic transport aircraft design is of primary importance in future air transportation. Concorde, a former supersonic transporter, had flown in the past since 1969; yet, it retired in 2003 due to its inefficiency and environmental impacts. Nowadays, academic and industrial supersonic airliner projects have been focusing on reducing the sonic boom loudness so that supersonic civil aviation can rejuvenate over land. [1–7]. In this concept, the aircraft geometry has a substantial influence on shock formations as well as the ground pressure signature. The mandated sonic boom loudness level by aviation regulations can be reached by optimizing the aircraft design which is a multi-disciplinary and demanding process. These bring the aerodynamic and structural design together with the consideration of the propulsion system integration, a crucial aspect of the design with an immense impact on environmental friendliness. Nonetheless, the computation to obtain near-field flow solutions with a realistic operating engine condition brings astronomically high costs in terms of time. Even though time-efficient flow solvers such as panel methods, and empirical approximations can be substitutes for computational fluid dynamics solvers, the physical accuracy they yield is unsatisfactory, which may lead to erroneous optimization results. Besides, the elastic structure deformation caused by the pressure distribution over the aircraft surface can also give rise to a change in the flow field, so it ought to be considered in the sonic boom evaluations although the multi-physics examined in this study, i.e. fluid-structure interaction, require complex and costly solutions. As a way out, multi-fidelity methods are embraced by the optimization community and exploited in such costly design processes. The multi-fidelity analysis leverages a small number of high-fidelity and a large number of low-fidelity data systematically through mathematical frameworks. The main objective is to dramatically reduce computational and design expenses while keeping the physical accuracy

*Professor, Faculty of Aeronautics and Astronautics, AIAA Associate Fellow
†Graduate Student, Research Assistant, AeroMDO Lab, Faculty of Aeronautics and Astronautics
‡Graduate Student, Research Scholar, AeroMDO Lab, Faculty of Aeronautics and Astronautics
§Graduate Student, Research Scholar, AeroMDO Lab, Faculty of Aeronautics and Astronautics
¶Graduate Student, Research Assistant, AeroMDO Lab, Faculty of Aeronautics and Astronautics
‖Graduate Student, Research Assistant, AeroMDO Lab, Faculty of Aeronautics and Astronautics

as high as the high-fidelity resources. The literature offers numerous research incorporating multi-fidelity methods into computational frameworks [8–14].

This study is ongoing research and intends to find a sought-after supersonic airliner geometry including outer mold line and wing structures with the assistance of multi-fidelity optimization methods. The genetic algorithm, a gradient-free optimization method, is coupled with the CoKriging surrogate modeling tool in order to minimize the need for computational resources. In addition, the aircraft fuselage and wings are parametrized using 20 variables in total using Engineering Sketch Pad[15], an open-source parametric modeling tool. Geometry and grid generation, flow solution, fluid-structure interaction, sonic boom propagation, and post-processing are coupled with an in-house script to generate a dataset.

The paper is described as follows. Section II introduces the formulation of near-field, sonic boom propagation, fluid-structure interaction, multi-fidelity surrogate modeling. In Section III, the selected baseline geometry and parametrization are explained, and then near-field, fluid-structure, and far-field solutions for baseline geometry are depicted in this section. Eventually, Section III provides the obtained results of the optimization study and Section IV presents the concluding remarks and future work.

II. Methodology

This section introduces the theoretical background of the considered multi-fidelity and multi-disciplinary design optimization study for a supersonic transport aircraft. First, near-field flow and far-field acoustics solution formulations are introduced. Then, sonic boom propagation and fluid-structure interaction methodologies exploited in this study are explained. Finally, data generation and multi-fidelity optimization processes are presented.

A. Near-Field Solution

In the sonic boom theory, a supersonic aircraft is assumed as a moving acoustic source that creates pressure waves. Therefore, to be able to solve wave propagation in the atmosphere, a near-field pressure signature must be obtained near the aircraft. A diagram that illustrates the sonic boom propagation process is shown in Figure 1. Due to the acoustic source assumption in the sonic boom calculations, this near field pressure signature must be taken from at least 2 or 3 body lengths away from the aircraft that serves as an initial source signal for the sonic boom propagation. Therefore, accurate prediction of near-field pressure signature is essential for the sonic boom loudness calculation.

In this study, the SU2 [16] code is used as the high-fidelity analysis solver. SU2 is an open-source unstructured multi-physics and design software that was developed by Stanford University - Aerospace Design Laboratory (ADL). SU2 is a robust and reliable CFD code for supersonic flow analysis. In addition, there are several studies for low boom analysis performed with SU2. This study is performed with a steady Euler solution with multi-grid methods. In the study, a hybrid mesh that consists of structured and unstructured mesh together was used due to the ease of creating meshes as in AIAA Sonic Boom Prediction Workshops (SBPW) [17].

B. Sonic Boom Prediction

The sonic boom propagation problem can be reduced to three main steps as illustrated in Figure 1; near-field calculation, far-field propagation, and loudness calculation. As a result of the flow analysis, the pressure change due to the shock waves caused by the geometry of the aircraft can be measured at distances close to the aircraft. The measured pressure changes are called near-field pressure signatures. A 1-dimensional lossy wave equation that contains the effect of thermoviscous attenuation and vibrational relaxation of O_2 and N_2, named augmented Burgers equation Eq. 1, is solved numerically in a ray tube coordinate system. The path of this horn-shaped ray tube can be calculated by the linear geometric acoustics method that allows for the stratified and windy atmosphere.

$$\frac{\partial P}{\partial \sigma} = P\frac{\partial P}{\partial \tau} + \frac{1}{\Gamma}\frac{\partial^2 P}{\partial \tau^2} + \sum_{\nu} C_\nu \frac{\frac{\partial^2}{\partial \tau^2}}{1+\theta_\nu \frac{\partial}{\partial \tau}} P - \frac{\frac{\partial}{\partial \sigma}A}{2A}P + \frac{\frac{\partial}{\partial \sigma}(\rho_0 c_0)}{2\rho_0 c_0}P \tag{1}$$

After the numerical solution of the wave equation from near-field to ground, the perceived loudness in decibels (PLdB) can be calculated from the ground signature.

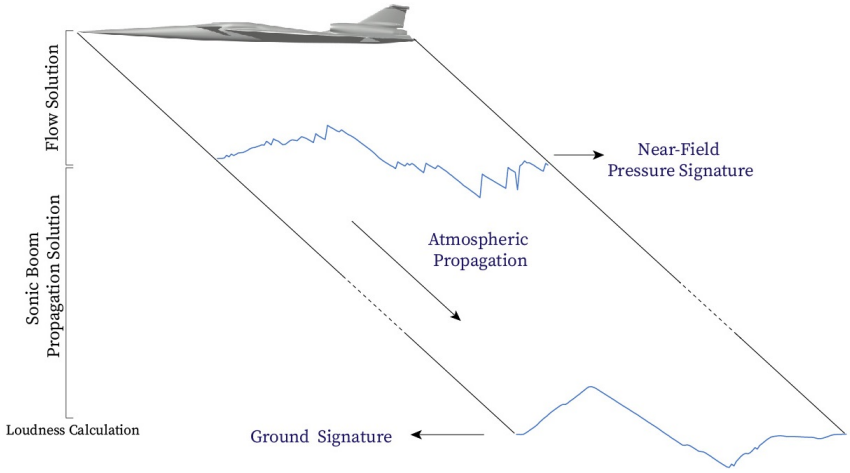

Fig. 1 Sonic boom prediction process [14].

In this study, a well-known sonic boom propagation tool developed by NASA Langley Research Center, sBOOM, is used as a wave propagation program [18]. For the perceived loudness calculation, USU Aero Lab's PyLdB [19] code is implemented.

C. Fluid-Structure Interaction Analysis

An elastic structure coupled with a fluid may deform in response to the pressure exerted. The deformation alters the flow-field. The pressure on the structure changes together with the changing flow-field, and this coupling is true across iterations. In this study, fluid-structure interaction analysis is performed to observe the effect of this change in the flow field on the sonic boom. For static aeroelasticity, accurate deformation calculations are crucial. Therefore, estimating wing tip displacement and researching fluid-structure interaction mostly employ computational approaches for fluid-structure interaction (FSI) analysis. For high-fidelity FSI analysis in this work, the open-source SU2 multi-physics tool with proven coupling capabilities is employed [20–22]. In the current study, a finite volume-based compressible Euler flow solver and a finite element-based materially non-linear (Neo Hookean) solid mechanical solver are coupled in SU2.

Moving boundaries and grid deformation are necessary for FSI. Structure, fluid, and mesh are the three domains used to handle fluid-structure interaction simulations in SU2. Each domain is governed by respective constitutive equations that interact over a shared interface [23]. It is possible to transmit displacement from the structure to the field domain as needed by using the mesh domain as a separate field. To track the deformation of the mesh, a mesh movement problem must be defined. In a mesh problem, the fictitious stiffness matrix times the vector of nodal mesh displacements equals the fictitious forces enforcing the boundary displacements. The mesh deformation is taken into account while updating the fluid problem. As a result, the governing equation is modified using the Arbitrary Lagrangian-Eulerian (ALE) framework for the fluid domain.

The fluid-structural interaction analysis is performed iteratively in the time step using the Block Gauss-Seidel method until a tolerance requirement is satisfied.

D. Dataset Generation

The design optimization study of a supersonic aircraft carried out within this project's scope requires a number of fluid, finite elements, and aeroacoustic analyses. An in-house Python script is developed to automatize the dataset generation process. Each analysis to be done has several stages, which can be listed in order as follows:

1) Parametric geometry generation
2) Numerical discretization
3) Simulations
4) Post-processing

First, the parametric geometry generation process is implemented using an open-source geometry modeling tool Engineering Sketch Pad [15] in the developed script. This process consists of two stages: wing-body configuration for

flow solutions and wing geometry with an inner structure for fluid-structure interaction, which is explained in Section III.A in detail. After that, flow domain discretization is performed for design updates at each iteration. At this step, three different scripts are employed for flow domain discretization and finite element method. Using the developed code, the user can easily set the parameters such as computational domain size and element length. The discretized flow domains have two different mesh structures: unstructured finer core region and structured far-field region. In this work, the low-fidelity solution domains consist of 1.2 million elements size while the high-fidelity solutions go up to 12.5 million elements size.

Table 1 Descriptive statistics of the generated MF sonic boom dataset.

	Minimum		Maximum		Mean		Median		Standard Deviation	
Parameter	**LF**	**HF**	**LF**	**HF**	**LF**	**HF**	**LF**	**HF**	**LF**	**HF**
Drag coefficient (C_D)	0.006690	0.006273	0.009549	0.008758	0.008071	0.007488	0.008028	0.007441	0.000486	0.000419
Lift coefficient (C_L)	0.071646	0.064479	0.115155	0.102954	0.093490	0.085454	0.093194	0.085318	0.006832	0.006168
Loudness value ($PLdB$)	89.18976	88.11422	95.33292	91.81154	91.13838	90.47507	91.18173	90.47525	0.581237	0.624368
Weight (W)	58486.90	59529.36	65466.86	65064.42	62427.60	62286.35	62458.86	62319.37	1076.406	1154.301

In this framework, the SU2 multi-physics flow solver is exploited for both low- and high-fidelity simulations using Euler equations. Since the flow conditions are kept constant, the same numerical methods and a configuration file are utilized for all generated models. In the data extraction part, open-source ParaView [24] post-processing tool is preferred to read and convert data from solution files. Furthermore, Halton quasi-random sampling scheme [25] is employed to obtain high- and low-fidelity sampling space within the range of design parameters depicted in Table 2. In total, 892 high-fidelity and 301 low-fidelity simulations are generated, which is shown in Fig. 2 for all desired output parameters: aerodynamic coefficients (C_D, C_L), loudness value ($PLdB$), and wing weight (W). In addition, the descriptive statistics of the generated multi-fidelity dataset are presented in Table 1. Finally, the embraced flowchart for multi-fidelity data generation and optimization study is illustrated in Figure 3.

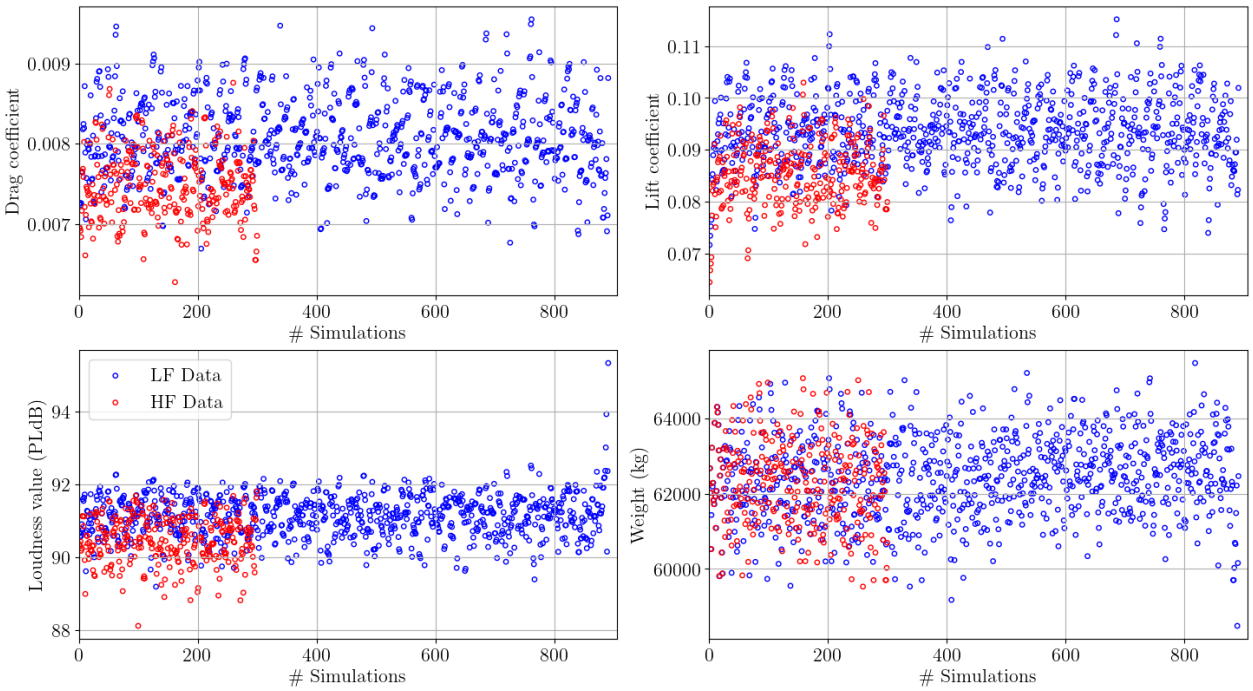

Fig. 2 Generated MF sonic boom dataset.

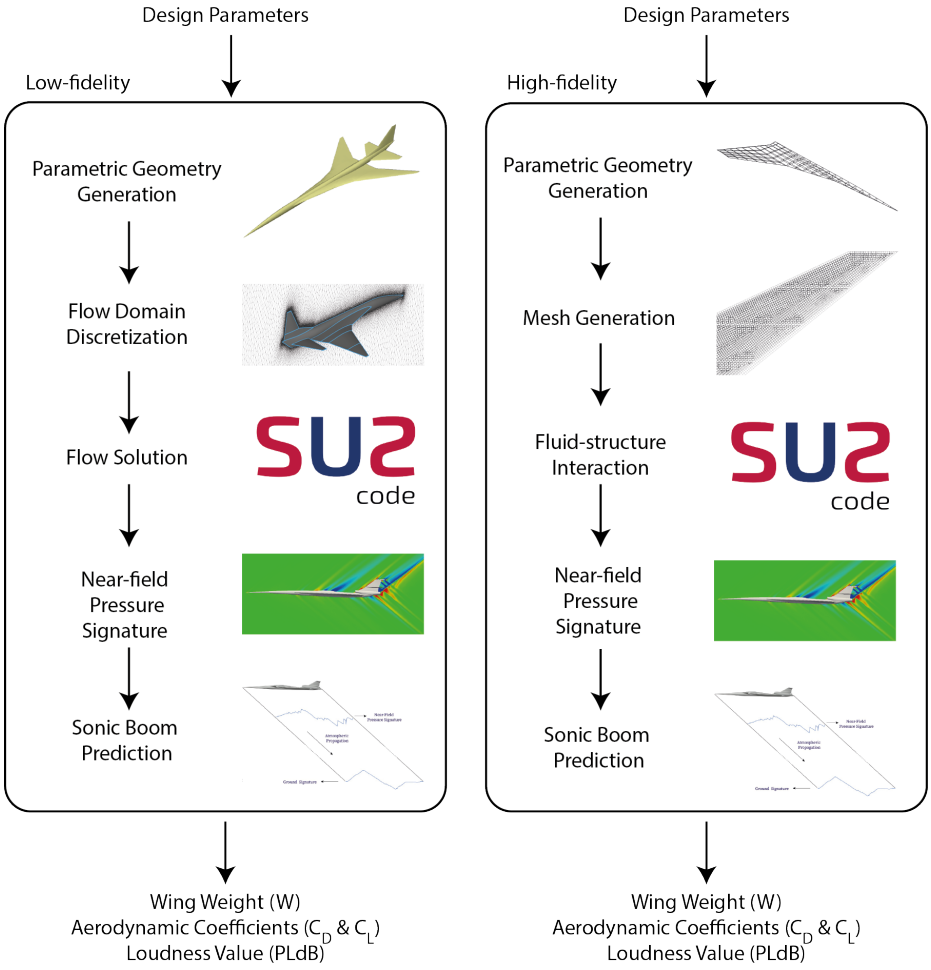

Fig. 3 Flowchart of multi-fidelity optimization study.

E. Multi-Fidelity Surrogate Modeling - Regression CoKriging Method

The primary concept underlying the CoKriging method provided in this work is based on the linear auto-regression data-fusion scheme proposed by Kennedy and O'Hagan. The auto-regression approach, which is stated as Eq. (2), accepts that any errors are wholly attributable to the low-fidelity analysis program and that the simulation of the high-fidelity analysis program is accurate.

$$\operatorname{cov}\left\{f_{hf}\left(\vec{x}^{(i)}\right), f_{lf}\left(\vec{x}^{(i)}\right) \mid f_{lf}\left(\vec{x}^{(i)}\right)\right\} = 0, \forall \vec{x} \neq \vec{x}^{(i)} \tag{2}$$

The main goal of the CoKriging method, as shown in Eq. (3), is to find a relationship between outcomes between low- and high-fidelity analysis programs. Here, the low-fidelity Gaussian process is denoted by $Z_{lf}(x)$, the scaling factor between low- and high-fidelity models is denoted by ρ, and the Gaussian process of differences between $Z_{lf}(x)$ and $Z_{hf}(x)$ is denoted by $Z_d(x)$.

$$Z_{hf}(\vec{x}) = \rho Z_{lf}(\vec{x}) + Z_d(\vec{x}) \tag{3}$$

The covariance between sampling points can be expressed as in Eq. (4). Here, R(.,.) is the correlation function, σ^2 model variance, $x^{(i)}, x^{(j)}$ are the i^{th} and j^{th} samples.

$$\operatorname{cov}\left(Z\left(x^{(i)}\right), Z\left(x^{(j)}\right)\right) = \sigma^2 R\left(x^i, x^j\right) \tag{4}$$

The typical correlation function used in the study is given in Eq. (5) and θ_l in the equation is the l^{th} correlation parameter.

$$R\left(x^i, x^j\right) = \exp\left[-\sum_{l=1}^{m} \theta_l \left|x_l^{(i)} - x_l^{(j)}\right|^2\right] \quad i, j = 1, 2, \ldots, N \tag{5}$$

The value at a position in the design space is regarded as though it were the realization of a stochastic process, and the covariance matrix for two different fidelity levels is calculated as in Eq. (6).

$$[\mathbf{C}] = \begin{bmatrix} \operatorname{cov}\{Z_{lf}(\mathbf{X_{lf}}), Z_{lf}(\mathbf{X_{lf}})\} & \operatorname{cov}\{Z_{hf}(\mathbf{X_{hf}}), Z_{lf}(\mathbf{X_{lf}})\} \\ \operatorname{cov}\{Z_{hf}(\mathbf{X_{hf}}), Z_{lf}(\mathbf{X_{lf}})\} & \operatorname{cov}\{Z_{hf}(\mathbf{X_{hf}}), Z_{hf}(\mathbf{X_{hf}})\} \end{bmatrix} \tag{6}$$

where,

$$\operatorname{cov}\{Z_{lf}(\mathbf{X_{lf}}), Z_{lf}(\mathbf{X_{lf}})\} = \hat{\sigma}_{lf}^2 \left[\boldsymbol{R}_{\mathbf{lf}}\left(\mathbf{X_{lf}}, \mathbf{X_{lf}}\right) + \mathbf{I}_{\left(N_{lf} \times N_{lf}\right)} \lambda_{lf}\right], \tag{7}$$

$$\operatorname{cov}\{Z_{hf}(\mathbf{X_{hf}}), Z_{lf}(\mathbf{X_{lf}})\} = \rho \hat{\sigma}_{lf}^2 \left[\boldsymbol{R}_{\mathbf{lf}}\left(\mathbf{X_{lf}}, \mathbf{X_{hf}}\right) + \begin{pmatrix} \mathbf{0}_{\left(N_{lf} - N_{hf} \times N_{hf}\right)} \\ \mathbf{I}_{\left(N_{hf} \times N_{hf}\right)} \end{pmatrix} \lambda_{lf}\right] \tag{8}$$

$$\operatorname{cov}\{Z_{hf}(\mathbf{X_{hf}}), Z_{lf}(\mathbf{X_{lf}})\} = \rho \hat{\sigma}_{lf}^2 \left[\boldsymbol{R}_{\mathbf{lf}}\left(\mathbf{X_{hf}}, \mathbf{X_{lf}}\right) + \begin{pmatrix} \mathbf{0}_{\left(N_{hf} \times N_{lf} - N_{hf}\right)} & \mathbf{I}_{\left(N_{hf} \times N_{hf}\right)} \end{pmatrix}\right) \lambda_{lf}\right], \tag{9}$$

$$\operatorname{cov}\{Z_{hf}(\mathbf{X_{hf}}), Z_{hf}(\mathbf{X_{hf}})\} = \rho^2 \hat{\sigma}_{lf}^2 \left[\boldsymbol{R}_{\mathbf{lf}}\left(\mathbf{X_{hf}}, \mathbf{X_{hf}}\right) + \mathbf{I}_{\left(N_{hf} \times N_{hf}\right)} \lambda_{lf}\right] + \hat{\sigma}_d^2 \left[\boldsymbol{R}_{\mathbf{d}}\left(\mathbf{X_{hf}}, \mathbf{X_{hf}}\right) + \mathbf{I}_{\left(N_{hf} \times N_{hf}\right)} \lambda_d\right] \tag{10}$$

The covariance matrix contains $\mathbf{R_{lf}}$ and $\mathbf{R_d}$ correlation functions, and these correlation functions contain unknown hyper parameters $(\theta_{lf}, \theta_d, \lambda_{lf}, \lambda_d)$. These parameters need to be determined using parameter estimation methods. In this study, the use of the maximum likelihood parameter estimation method is preferred for the estimation of hyperparameters.

The hyper-parameters θ_{lf}, and λ_{lf} are obtained by maximizing the maximum log-likelihood function given in Eq. 11 to set-up Kriging surrogate model of low-fidelity analysis program.

$$-\frac{N_{lf}}{2} \ln\left(\hat{\sigma}_{lf}^2\right) - \frac{1}{2} \ln\left|\det\left(\left[\boldsymbol{R}_{\mathbf{lf}}\left(\boldsymbol{X}_{\mathbf{lf}}, \boldsymbol{X}_{\mathbf{lf}}\right) + \mathbf{I}_{\left(N_{lf} \times N_{lf}\right)} \lambda_{lf}\right]\right)\right| \tag{11}$$

The difference vector should be defined as in Eq. (12) in order to model deviation between high- and low-fidelity analysis program.

$$\vec{d} = \vec{Y}_{hf} - \rho\ f_{lf}\left(\boldsymbol{X_{hf}}\right) \tag{12}$$

By maximizing Eq. (13), the other unknown hyperparameters required to calculate the deviation between the low- and high-fidelity analysis program are obtained.

$$-\frac{N_{hf}}{2} \ln\left(\hat{\sigma}_d^2\right) - \frac{1}{2} \ln\left|\det\left(\left[\boldsymbol{R}_{\mathbf{d}}\left(\boldsymbol{X}_{\mathbf{hf}}, \boldsymbol{X}_{\mathbf{hf}}\right) + \mathbf{I}_{\left(N_{hf} \times N_{hf}\right)} \lambda_d\right]\right)\right| \tag{13}$$

Together with the determination of the hyper-parameters, the prediction of CoKriging multi-fidelity surrogate model is computed as in Eq. (14).

$$\tilde{f}_{hf}\left(\vec{x}_{new}\right) = \hat{\mu} + \vec{c}^{\mathrm{T}} [\mathbf{C}]^{-1} (\vec{Y} - \vec{1}\hat{\mu}) \tag{14}$$

The $\vec{c}$ in Eq. (14) is the correlation function between training data sets and the design variables to be predicted, and multi-fidelity trend function value in the equation is calculated as $\hat{\mu} = \mathbf{1}^{\mathrm{T}} [\mathbf{C}]^{-1} \vec{Y} / \mathbf{1}^{\mathrm{T}} [\mathbf{C}]^{-1} \mathbf{1}$.

$$\vec{c} = \begin{bmatrix} \hat{\rho} \hat{\sigma}_{lf}^2\ \vec{R}_{lf}\left(\boldsymbol{X}_{lf}, \vec{x}_{new}\right) \\ \hat{\rho}^2 \hat{\sigma}_{lf}^2\ \vec{R}_{lf}\left(\boldsymbol{X}_{lf}, \vec{x}_{new}\right) + \hat{\sigma}_d^2\ \vec{R}_d\left(\boldsymbol{X}_{lf}, \vec{x}_{new}\right) \end{bmatrix} \tag{15}$$

Additionally, the mean-squared error of the CoKriging model can be estimated as in Eq. (16).

$$\hat{s}^2(x_{new}) = \hat{\rho}^2 \hat{\sigma}_{lf}^2 + \hat{\sigma}_d^2 - \vec{c}^{\mathrm{T}} [\mathbf{C}]^{-1} \vec{c} \tag{16}$$

III. Application and Results

In this section, the results of multi-fidelity sonic boom minimization for a commercial supersonic transport aircraft are highlighted. First, the case description is comprehensively explained, then near-field, fluid-structure interaction, and far-field acoustics solutions for baseline airliner configuration are provided. Finally, multi-fidelity optimization study results are discussed.

A. Case Description

This section documents parametric geometry generation and baseline configuration solutions from SU2 and sBOOM for both low- and high-fidelity methods. First, baseline airliner wing-fuselage and nacelle configuration, and its geometric information are presented in detail. After that, flow, fluid-structure, and sonic boom solutions are provided, respectively.

1. Baseline Geometry and Parametrization

The embraced baseline geometry for a low-boom supersonic transport aircraft is approximately regenerated using the planform information in the study carried out by Li and Geiselhart [1]. For parametric geometry generation, open-source computer program, Engineering Sketch Pad (ESP) [15], is employed for defining both outer mold line (OML) and wing inner structure. The baseline supersonic airliner configuration which has a 242 ft long fuselage and 98 ft wingspan is presented in Fig. 4

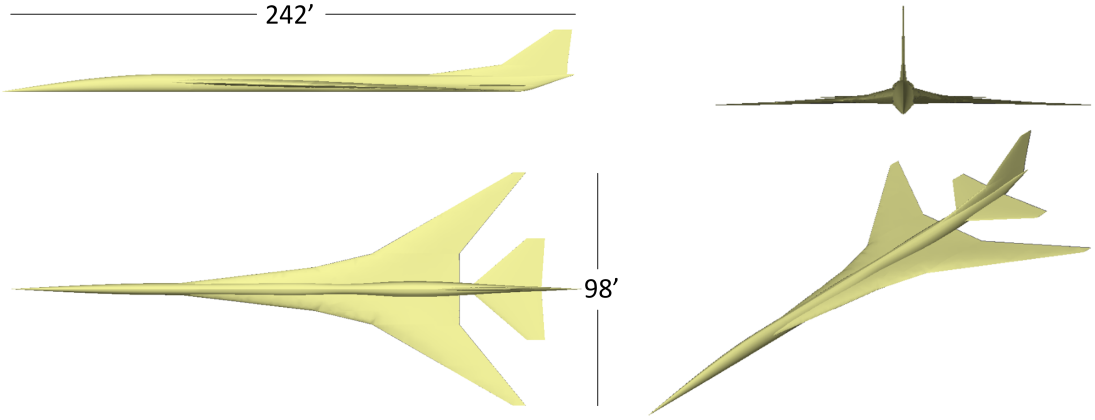

Fig. 4 Baseline airliner configuration.*

The baseline wing , horizontal, and vertical tail components consist of NACA 63-series airfoils. The lower and upper values for design optimization study are listed in Table 2. The fuselage is parametrized with 8 design variables exhibited in Fig. 5 (d_i: fuselage cross section width parameter at station x_i, x_i: fuselage cross section location along x coordinate, z: fuselage noze z-axis position, and α: angle of attack).

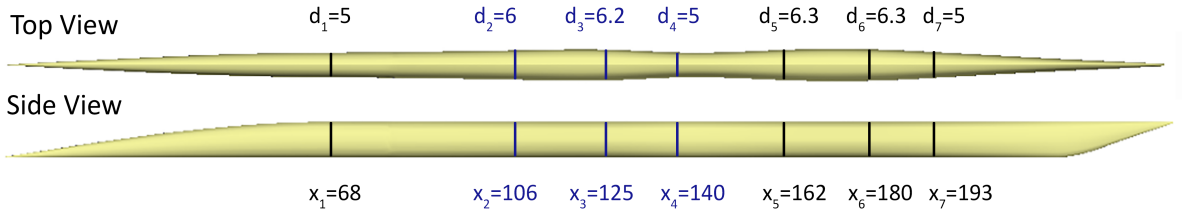

Fig. 5 Baseline fuselage with geometry parameters.

On the other hand, the baseline with four partitions along the span comprises 9 design variables shown in Fig. 6

(s_i: span length at ith wing section, Λ_i: sweep angle at ith wing section, θ_i: twist angle of an airfoil at span location y_i, and c_5: chord length at the wing tip section).

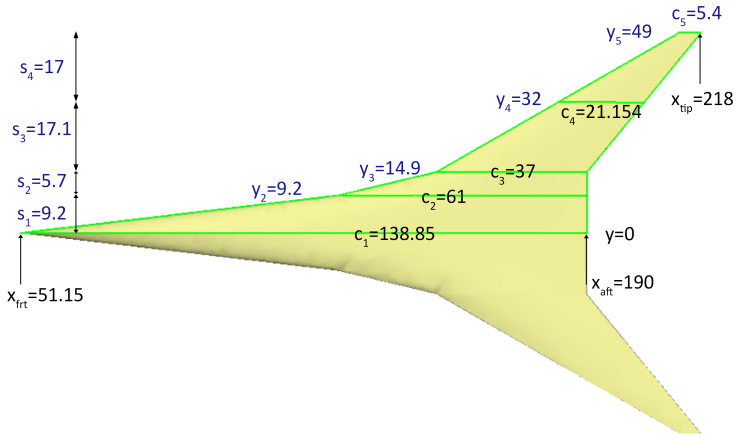

Fig. 6 Baseline wing with geometry parameters.

Finally, the horizontal tail is considered with 3 geometric design variables ($x_{frt_{(htail)}}$: root airfoil section leading edge point along x-axis, Λ_{htail}: sweep angle at ith airfoil section, and β_{htail}: angle of incidence of the horizontal tail with respect to the fuselage).

Table 2 Geometry design variables.

Fuselage	$100 \leq x_2 \leq 110$	$5.1 \leq d_2 \leq 7$
	$120 \leq x_3 \leq 130$	$5.1 \leq d_3 \leq 7$
	$135 \leq x_4 \leq 150$	$5.1 \leq d_4 \leq 7$
	$-7.3/2 \leq z \leq 0$	$0.7 \leq \alpha \leq 0.8$
Wing	$5 \leq s_2 \leq 6$	$70 \leq \Lambda_2 \leq 75$
	$15 \leq s_3, s_4 \leq 18$	$60 \leq \Lambda_3 \leq 65$
	$5 \leq c_5 \leq 6$	$60 \leq \Lambda_4 \leq 65$
	$-0.5 \leq \theta_3, \theta_4, \theta_5 \leq 0.5$	
Horizontal Tail	$192 \leq x_{frt_{(htail)}} \leq 193.5$	$45 \leq \Lambda_{htail} \leq 55$
	$-0.5 \leq \beta_{htail} \leq 0.5$	

In our previous optimization study [26], three-stage optimization was taken into account to reach optimum airliner geometry with nacelle configuration. Using the design parameters in Table 3 (except angle of attack), first we implemented a single-fidelity optimization study to determine the optimum OML structure of the aircraft aerodynamically. Then, the optimum geometry from this study was considered as the baseline geometry and an optimization study was repeated to find the optimum inner structure and material properties for this optimum configuration. In the second optimization stage, we considered the design parameters: spar & rib thickness, Young modulus, Poisson ratio, and material density to achieve minimum wing displacement, which is listed in Table 3. Eventually, an optimization study was carried out to obtain the optimum nacelle location of the aforementioned airliner geometry. The optimum nacelle x- and y-locations are exhibited in Table 4.

In our current optimization study, now we consider angle of attack value as a design parameter. Also, we increase the fidelity level of the study to diminish computational effort and costs.

*All design parameters are in feet.

Table 3 Structural parameters obtained from previous optimization study[26].

Parameter	Value
Rib thickness (ft)	0.1394
Spar thickness (ft)	0.1394
Young modulus (GPa)	86.775
Poisson ratio	0.3149
Material density (kg/m^3)	2500.5161

Table 4 Nacelle location obtained from previous optimization study[26].

Parameter	Value
x-position wrt origin (ft)	52.06835938
y-position wrt origin (ft)	3.89300412

Moreover, a nacelle configuration is designed and integrated based on the inlet and outlet conditions of the F404 engine, which was regenerated in our previous study [27], and is shown in Fig. 7.

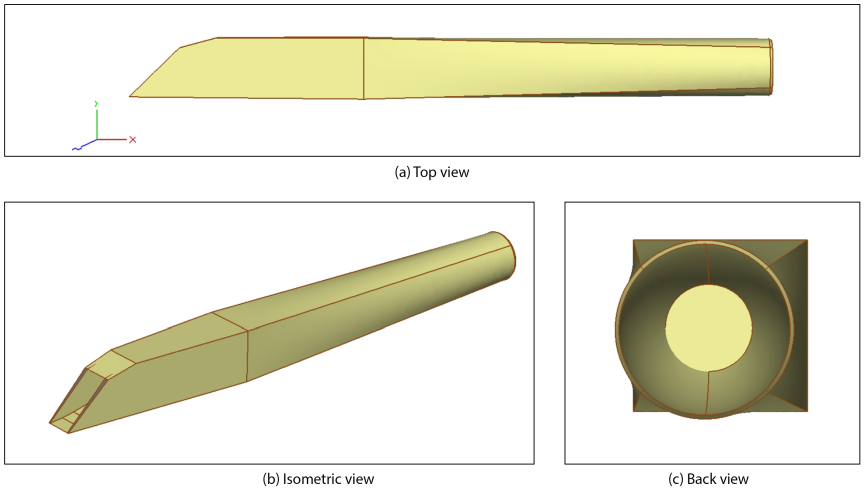

Fig. 7 Considered three-ramp nacelle geometry.

2. Near-field Fluid-Structure Interaction Solution

Two levels of fidelity are considered such that the rigid case is a low-fidelity solution and the aeroelastic case is a high-fidelity. First, the supersonic flow solution where the Mach number equals 1.6 must be performed with SU2 for the baseline geometry. The near-field analysis is conducted at a 55000 ft altitude and 0.7 degree angle of attack. In SU2, 10^{-7} convergence criterion is selected for the RMS density. A solution domain is created with 12.5 million elements for both unstructured and structured parts as shown in Fig. 8. The size of the solution domain is determined accordingly to be able to extract pressure signature at 2 body lengths below the aircraft.

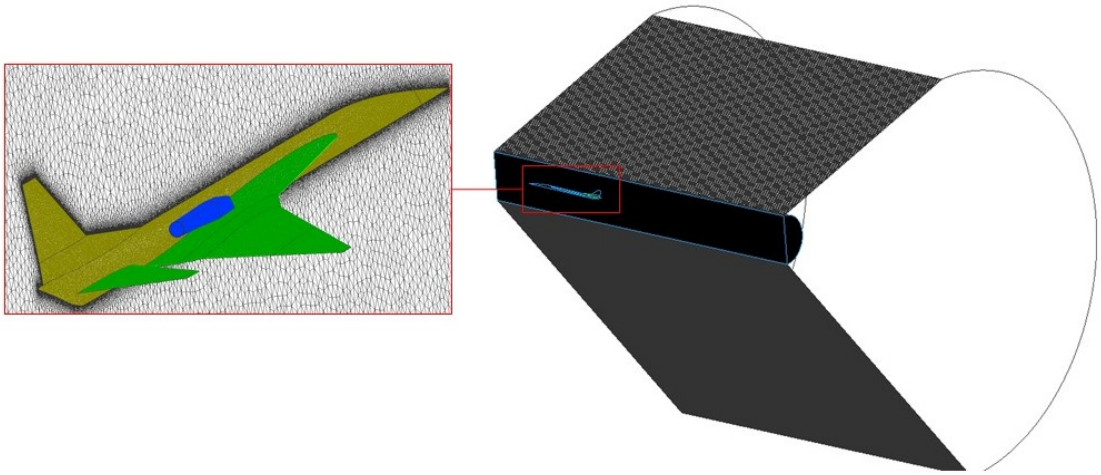

Fig. 8 CFD solution domain.

A rigid case takes approximately 1 hour while an aeroelastic case lasts 4 hours with parallel libraries with 128 cores. The pressure coefficient distribution over the aircraft geometries as well as the symmetry plane are depicted in Fig. 9a while Fig. 9b shows near-field pressure signature for both rigid and aeroelastic cases.

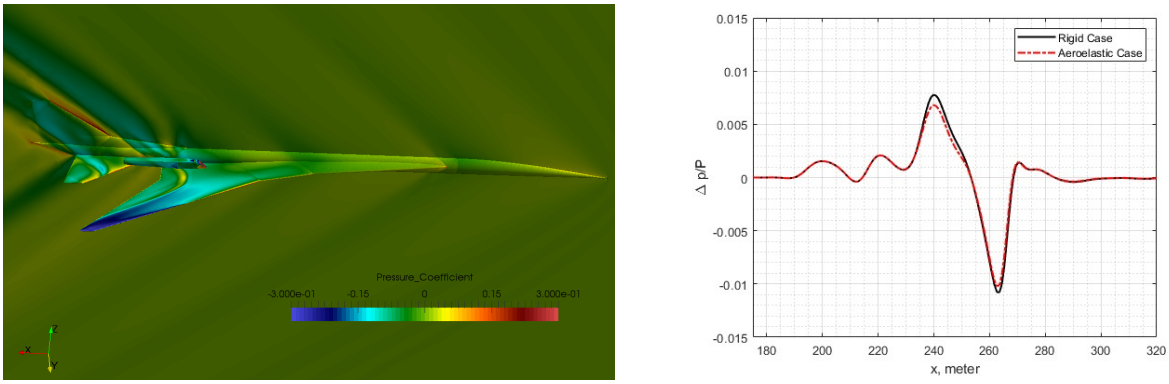

(a) Top view **(b) Bottom view**

Fig. 9 Result of near-field CFD solution.

As a high-fidelity solution for the baseline geometry, fluid-structure interaction analysis is performed with the SU2 multi-pyhsics solver. Along with the flow domain which has 12.5 million elements, the structural domain is generated by using the 1.5 million elements for the wing structural model, which is modeled as solid. While the flow conditions are used the same as rigid cases, the parameters in Tab. 3 are employed for structural inputs. After completing FSI computations, the near-field pressure signature is compared with the rigid solution in Fig. 9b, while the displacement distribution on the wing is depicted in Fig. 10.

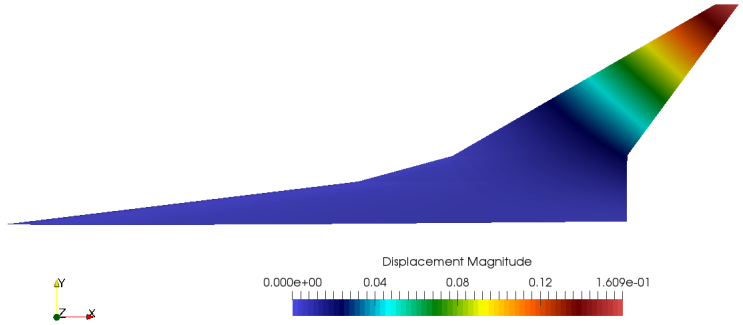

Fig. 10 Displacement distribution.

3. Sonic Boom Solution

After obtaining the near-field pressure signature, they are entered into sBOOM code for propagation to the ground. Flight altitude is set to 55000 ft with a standard atmosphere without wind. 10000 points are used to represent waveform during propagation. We performed all analyzes for on-track conditions where the azimuth angle equals zero. Resultant ground signatures are presented in Fig. 11.

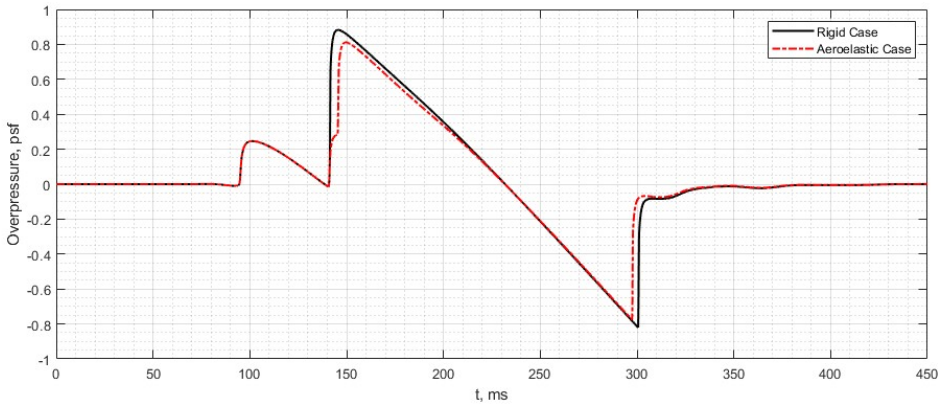

Fig. 11 Ground signature comparison for rigid and aeroelastic cases of baseline geometry.

B. Multi-fidelity Sonic Boom Minimization

In the optimization study, the goal is to achieve geometry that produces a minimal sonic boom value. However, it is not preferred that the final design have lower lift and higher drag, weight values than the base geometry. As a result, in optimization research, the lift, drag, and weight values of the base geometry are defined as constraints.

$$
\begin{aligned}
\min_{s \in S} \quad & \Delta P(s) \\
\text{subject to} \quad & g_1(s) = D(s) - D_{base} \leq 0, \quad g_1(s) \in \Re \\
& g_2(s) = L_{base} - L(s) \leq 0, \quad g_2(s) \in \Re \\
& g_3(s) = W(s) - W_{base} \leq 0, \quad g_3(s) \in \Re \\
& S = \{s \in \Re,\ s_L \leq s \leq s_U\}
\end{aligned}
\tag{17}
$$

The optimization problem is described in Eq. (17), and in order to handle the constraints, the optimization study is conducted by incorporating the constraints in the objective function using the penalty function method as shown in Eq. (18).

$$\min_{s \in S} \quad \Delta P(s) + k_1 p_L(L(s), L_{base}) + k_2 p_D(D(s), D_{base}) + k_3 p_w(W(s), W_{base}) \tag{18}$$

Penalty terms are determined by normalizing the deviation from the performance parameters of the baseline geometry using the maximum and minimum values in the data set as in Eq. (19), (20), and (21) where $k_1 = 1000$ and $k_2 = k_3 = 100$.

$$p_L(L(s), L_{base}) = \begin{cases} 0 & \text{if } L(s) \geq L_{base} \\ \frac{L_{base} - L(s)}{L_{max} - L_{min}} & \text{if } L(s) < L_{base} \end{cases} \tag{19}$$

$$p_D(D(s), D_{base}) = \begin{cases} \frac{D(s) - D_{base}}{D_{max} - D_{min}} & \text{if } D(s) \geq D_{base} \\ 0 & \text{if } D(s) < D_{base} \end{cases} \tag{20}$$

$$p_W(W(s), W_{base}) = \begin{cases} \frac{W(s) - W_{base}}{W_{max} - W_{min}} & \text{if } W(s) \geq W_{base} \\ 0 & \text{if } W(s) < W_{base} \end{cases} \tag{21}$$

The performance parameters of the optimum and base geometries are presented in Table 5. With these results, 8.48% reduction in ΔP is obtained by shape optimization.

Table 5 Comparison of optimum and base geometry parameters.

Metric	Base Geometry	Optimum Geometry	Improvement (%)
ΔP (PLdB)	97.28	89.03	8.48
L (N)	778388.12	781344.89	0.37
D (N)	75619.75	64697.86	14.44
W (kg)	62250.48	59700.16	4.09

Optimum and baseline geometries are shown in Fig 12 and 13.

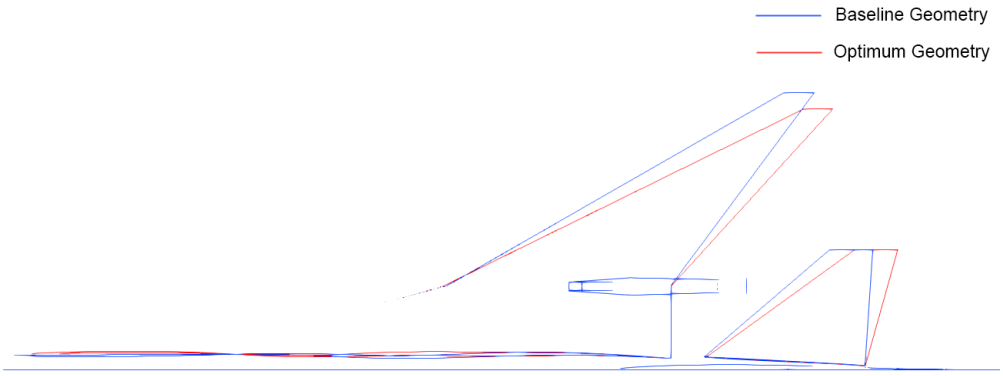

Fig. 12 Planform view of baseline and optimum airliner configurations.

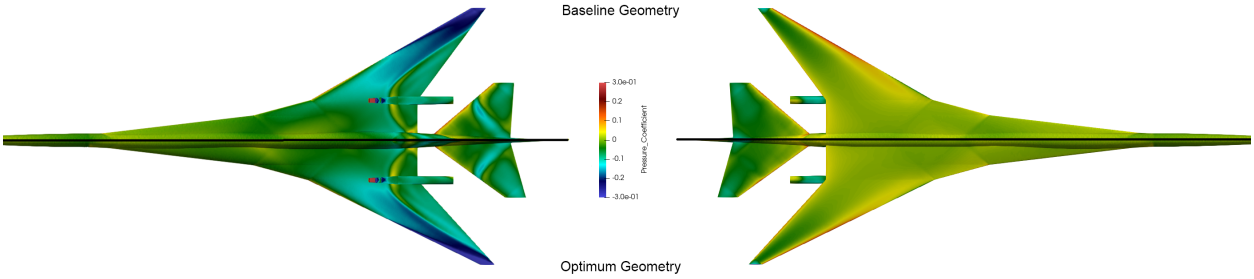

Fig. 13 C_P distribution on the upper (left) and lower (right) surface of baseline and optimum geometry.

IV. Conclusion and Future Work

In this study, the preliminary results of an ongoing research in multi-fidelity and multi-disciplinary design optimization are presented for a commercial supersonic aircraft configuration. In this framework, for parametric geometry generation, the open-source ESP program is exploited. Then, rigid and aeroelastic flow solutions around a supersonic aircraft are solved using the SU2 suite for low- and high-fidelity levels, respectively. Following near-field analysis, sonic boom propagation is calculated to the ground using the NASA sBOOM program. The study proceeded with a multi-fidelity surrogate-based optimization process to reach the sought-after optimum shape for the outer mold geometry. At this stage, multi-fidelity surrogate modeling and optimization studies are performed by using the in-house CoKriging and genetic algorithm codes of ITU AeroMDO Lab, respectively. Finally, satisfactory optimization results are obtained from the embraced multi-fidelity framework; nonetheless, further improvements and studies are required to achieve the desired sonic boom value for the supersonic airliner configuration. As a result, a 8.48% reduction in PLdB (perceived loudness in decibels) is achieved by the current shape optimization process for a commercial supersonic aircraft model with a complex geometry. The on-going study will be continued with implementation of additional geometric design variables via new parametrization approaches and also the surrogate based optimization process will be further assisted by benefits of active sampling techniques.

Acknowledgement

All authors would like to express their gratitude to TUBITAK for the research grant provided under the 218M471 TUBITAK 1001 project titled as "Development of Multi-fidelity and Multidisciplinary Methodologies Integrating Sonic Boom, Aeroelasticity, and Propulsion Systems for Supersonic Aircraft Design."

The first author would like to thank NASA Langley Research Center for distributing the sBOOM sonic boom prediction code internationally for academic research.

References

[1] Li, W., and Geiselhart, K., "Integration of Low-Fidelity MDO and CFD-Based Redesign of Low-Boom Supersonic Transports," *AIAA Journal*, Vol. 59, No. 10, 2021, pp. 3923–3936. https://doi.org/10.2514/1.j060368, URL https://doi.org/10.2514/1.j060368.

[2] Lawrence, J. P., Hutchinson, R. J., and Joiner, K. F., "Conceptual aerodynamic design of an executive supersonic passenger aircraft – ESPA," *Proceedings of the Institution of Mechanical Engineers, Part G: Journal of Aerospace Engineering*, Vol. 236, No. 5, 2021, pp. 923–937. https://doi.org/10.1177/09544100211025102, URL https://doi.org/10.1177/09544100211025102.

[3] Jim, T. M. S., Faza, G. A., Palar, P. S., and Shimoyama, K., "Bayesian Optimization of a Low-Boom Supersonic Wing Planform," *AIAA Journal*, Vol. 59, No. 11, 2021, pp. 4514–4529. https://doi.org/10.2514/1.j060225, URL https://doi.org/10.2514/1.j060225.

[4] Sun, Y., Smith, H., and Chen, H., "Conceptual Design of Low-Boom Low-Drag Supersonic Transports," *AIAA AVIATION 2020 FORUM*, American Institute of Aeronautics and Astronautics, 2020. https://doi.org/10.2514/6.2020-2635, URL https://doi.org/10.2514/6.2020-2635.

[5] Ban, N., Yamazaki, W., and Kusunose, K., "Low-Boom/Low-Drag Design Optimization of Innovative Supersonic Transport

Configuration," *Journal of Aircraft*, Vol. 55, No. 3, 2018, pp. 1071–1081. https://doi.org/10.2514/1.c034171, URL https://doi.org/10.2514/1.c034171.

[6] Ordaz, I., and Li, W., "Approximation of Off-Body Sonic-Boom Analysis for Low-Boom Conceptual Design," *Journal of Aircraft*, Vol. 53, No. 1, 2016, pp. 14–19. https://doi.org/10.2514/1.c033159, URL https://doi.org/10.2514/1.c033159.

[7] H, X., and S, C., "The Research of Supersonic Aircraft Low Sonic Boom Configuration Design and Optimizations," *Journal of Aeronautics &amp Aerospace Engineering*, Vol. 5, No. 2, 2016. https://doi.org/10.4172/2168-9792.1000165, URL https://doi.org/10.4172/2168-9792.1000165.

[8] Liu, Y., Chen, S., Wang, F., and Xiong, F., "Sequential optimization using multi-level cokriging and extended expected improvement criterion," *Structural and Multidisciplinary Optimization*, Vol. 58, No. 3, 2018, pp. 1155–1173. https://doi.org/10.1007/s00158-018-1959-6.

[9] Keane, A. J., "Cokriging for Robust Design Optimization," *AIAA Journal*, Vol. 50, No. 11, 2012, pp. 2351–2364. https://doi.org/10.2514/1.j051391.

[10] Nagawkar, J., Leifsson, L. T., and Du, X., "Applications of Polynomial Chaos-Based Cokriging to Aerodynamic Design Optimization Benchmark Problems," *AIAA Scitech 2020 Forum*, American Institute of Aeronautics and Astronautics, 2020. https://doi.org/10.2514/6.2020-0542.

[11] March, A., Willcox, K., and Wang, Q., "Gradient-based multifidelity optimisation for aircraft design using Bayesian model calibration," *The Aeronautical Journal (1968)*, Vol. 115, No. 1174, 2011, p. 729–738. https://doi.org/10.1017/S0001924000006473.

[12] Cheng, K., Lu, Z., and Zhen, Y., "Multi-level multi-fidelity sparse polynomial chaos expansion based on Gaussian process regression," *Computer Methods in Applied Mechanics and Engineering*, Vol. 349, 2019, pp. 360–377. https://doi.org/10.1016/j.cma.2019.02.021.

[13] West, T. K., and Phillips, B. D., "Multifidelity Uncertainty Quantification of a Commercial Supersonic Transport," *Journal of Aircraft*, Vol. 57, No. 3, 2020, pp. 491–500. https://doi.org/10.2514/1.c035496.

[14] Demiroglu, Y., Yildiz, S., and Nikbay, M., "Multi-fidelity Sonic Boom Minimization of a Supersonic Aircraft by Parametric Wing Shape Design," *AIAA Scitech 2021 Forum*, American Institute of Aeronautics and Astronautics, 2021. https://doi.org/10.2514/6.2021-1009, URL https://doi.org/10.2514/6.2021-1009.

[15] Haimes, R., and Dannenhoffer, J., "The Engineering Sketch Pad: A Solid-Modeling, Feature-Based, Web-Enabled System for Building Parametric Geometry," *21st AIAA Computational Fluid Dynamics Conference*, American Institute of Aeronautics and Astronautics, 2013. https://doi.org/10.2514/6.2013-3073, URL https://doi.org/10.2514/6.2013-3073.

[16] Economon, T. D., Palacios, F., Copeland, S. R., Lukaczyk, T. W., and Alonso, J. J., "SU2: An open-source suite for multiphysics simulation and design," *AIAA Journal*, Vol. 54, No. 3, 2016, pp. 828–846. https://doi.org/10.2514/1.J053813.

[17] Park, M. A., and Nemec, M., "Nearfield Summary and Statistical Analysis of the Second AIAA Sonic Boom Prediction Workshop," *Journal of Aircraft*, Vol. 56, No. 3, 2019, pp. 851–875. https://doi.org/10.2514/1.c034866, URL https://doi.org/10.2514/1.c034866.

[18] Rallabhandi, S., "Advanced Sonic Boom Prediction Using Augmented Burger's Equation," *49th AIAA Aerospace Sciences Meeting*, American Institute of Aeronautics and Astronautics, 2011. https://doi.org/10.2514/6.2011-1278, URL https://doi.org/10.2514/6.2011-1278.

[19] Bolander, C. R., Hunsaker, D. F., Shen, H., and Carpenter, F. L., "Procedure for the Calculation of the Perceived Loudness of Sonic Booms," *AIAA Scitech 2019 Forum*, American Institute of Aeronautics and Astronautics, 2019. https://doi.org/10.2514/6.2019-2091, URL https://doi.org/10.2514/6.2019-2091.

[20] Sanchez, R., Kline, H. L., Thomas, D., Variyar, A., Righi, M., Economon, T. D., Alonso, J. J., Palacios, R., Dimitriadis, G., and Terrapon, V., "ASSESSMENT OF THE FLUID-STRUCTURE INTERACTION CAPABILITIES FOR AERONAUTICAL APPLICATIONS OF THE OPEN-SOURCE SOLVER SU2." *Proceedings of the VII European Congress on Computational Methods in Applied Sciences and Engineering (ECCOMAS Congress 2016)*, Institute of Structural Analysis and Antiseismic Research School of Civil Engineering National Technical University of Athens (NTUA) Greece, 2016. https://doi.org/10.7712/100016.1903.6597, URL https://doi.org/10.7712/100016.1903.6597.

[21] Sanchez, R., Palacios, R., Economon, T. D., Kline, H. L., Alonso, J. J., and Palacios, F., "Towards a Fluid-Structure Interaction Solver for Problems with Large Deformations Within the Open-Source SU2 Suite," *57th AIAA/ASCE/AHS/ASC Structures, Structural Dynamics, and Materials Conference*, American Institute of Aeronautics and Astronautics, 2016. https://doi.org/10.2514/6.2016-0205, URL https://doi.org/10.2514/6.2016-0205.

[22] Yildiz, S., Cakmak, E., Kara, E., and Nikbay, M., "UNCERTAINTY QUANTIFICATION OF AEROELASTIC SYSTEMS USING ACTIVE LEARNING GAUSSIAN PROCESS," 2021.

[23] Venkatesan-Crome, C., Gomes, P. C., and Palacios, R., "Optimal Compliant Airfoils Using Fully Non-Linear FSI Models," *AIAA Scitech 2019 Forum*, American Institute of Aeronautics and Astronautics, 2019. https://doi.org/10.2514/6.2019-1216, URL https://doi.org/10.2514/6.2019-1216.

[24] Ahrens, J. P., Geveci, B., and Law, C. C., "ParaView: An End-User Tool for Large-Data Visualization," *The Visualization Handbook*, 2005.

[25] Halton, J. H., "On the efficiency of certain quasi-random sequences of points in evaluating multi-dimensional integrals," *Numerische Mathematik*, Vol. 2, No. 1, 1960, pp. 84–90. https://doi.org/10.1007/bf01386213.

[26] Nikbay, M., Yildiz, S., Demiroglu, Y., Tekaslan, H. E., Cakmak, E., Kilic, D., and Imrak, R., "218M471 TUBITAK 1001 (The Scientific and Technological Research Council of Türkiye): Development of Multi-fidelity and Multidisciplinary Methodologies Integrating Sonic Boom, Aeroelasticity and Propulsion System for Supersonic Aircraft Design," Tech. rep., Istanbul Technical University, Sep. 2022.

[27] Imrak, R., Karaselvi, E., Tutkun, B., and Nikbay, M., *Exploration of Optimal Propulsion System Airframe Integration Design Concepts for a Low Boom Supersonic Aircraft*, 2021. https://doi.org/10.2514/6.2021-2469, URL https://arc.aiaa.org/doi/abs/10.2514/6.2021-2469.